# MTT Test and Time-lapse Microscopy to Evaluate the Antitumor Potential of Nucleoside Analogues

ALEXANDRA KISS[1], VIKTÓRIA BAKSA[1], MIKLÓS BEGE[2,3], LÁSZLÓ TÁLAS[1],
ANIKÓ BORBÁS[2], ILONA BERECZKI[2], GÁSPÁR BÁNFALVI[1] and GÁBOR SZEMÁN-NAGY[1]

[1]Department of Molecular Biotechnology and Microbiology, University of Debrecen, Debrecen, Hungary;
[2]Department of Pharmaceutical Chemistry, University of Debrecen, Debrecen, Hungary;
[3]MTA-DE Molecular Recognition and Interaction Research Group, University of Debrecen, Debrecen, Hungary

**Abstract.** *Background/Aim: Conventional viability tests, help to screen the cellular effects of candidate molecules, but the endpoint of these measurements lacks sufficient information regarding the molecular aspects. A non-invasive, easy-to-setup live-cell microscopic method served to in-depth analysis of mechanisms of potential anticancer drugs. Materials and Methods: The proposed method combining the MTT (3-(4,5-dimethylthiazol-2-yl)-2,5-diphenyltetrazolium bromide) test with time-lapse scanning microscopy (TLS), provided additional data related to the cell-cycle and the dynamic properties of cell morphology. Apoptotic and necrotic events became detectable with these methods. Results: Quantification of the results was assisted by image analysis of the acquired image sequences. After demonstrating the potential of the TLS method, a series of experiments compared the in vitro effect of a known and a newly synthesized nucleoside analogue. Conclusion: The proposed approach provided a more in-depth insight into the cellular processes that can be affected by known chemotherapeutic agents including nucleoside analogues rather than applying repeated individual treatments.*

Cell cultures in a carbon dioxide incubator can be observed continuously by photomicroscopy. The long-term scanning setup connected with the computer resulted in a custom made time-lapse scanning photomicroscopy (TLS) system. The spreading up of projection of real-time microscopy brought about time-lapse imaging video microscopy. With the help of video microscopy, individual cells and groups of cells in cell cultures can be observed up to several weeks; generally up to 7 days with one exposure/min temporal resolution. This method turned out to be feasible to examine adherent cells. The fate of individual mother cells, daughter cells, as well as populations and the cellular functions such as cell growth, cell division, viability, confluency could be measured. The effect of several cytotoxic agents on cell cultures has been investigated and offered quantitative evaluation suitable to observe characteristic changes of cells at individual and population levels. The long-term observation of cells was secured under physiological conditions by the photography of cells every minute (1). The results obtained by the qualitative method of TLS and evaluation of image analysis complemented by the (3-(4,5-dimethyl-thiazol-2-yl)-2,5-diphenyl-tetrazolium-bromide) (MTT) test broaden the knowledge of cytotoxicology.

The MTT test is based on the reduction of a tetrazolium salt and often used in *in vitro* toxicology experiments to judge the effect of xenobiotics on the viability and metabolic activity of cell cultures. The reduction of MTT turns the light yellow tetrazolium-salt to dark purple formazan that dissolved in DMSO can be determined spectrophotometrically. The reduction power of cells catalyzed by dehydrogenase enzymes forms NADPH from NADP. Under optimized conditions, the values of absorbances are proportional to the viability of cells. The MTT test was originally designed for eukaryotic cell lines then adapted to bacteria and fungi (2, 3).

By utilizing the MTT-test, one can estimate the effect of chemical compounds on the viability of cells. The test compares treated *versus* control cells and provides information at the population level whether or not cells are alive or dead. The information obtained by the inhibition of a substance at different concentrations is sufficient to determine its inhibitory concentration ($IC_{50}$). The image analysis of TLS uses the open-source image processing toolkit Image Fiji of NIH.

*Correspondence to:* Prof. Gaspar Banfalvi, Department of Molecular Biotechnology and Microbiology, University of Debrecen, 1 Egyetem Square, Debrecen 4010, Hungary. Tel: +36 52512900 ext. 62319, Fax: +36 52512925, e-mail: gaspar.banfalvi@gmail.com; bgaspar@unideb.hu

The $IC_{50}$ values suggested a combined analysis and further experiments that were performed by TLS. Cell cultures treated with a compound at its $IC_{50}$ concentration show the changes of specific processes that remained hidden by the MTT test. The TLS provides a visible insight into cell growth, answering the question of whether growth was inhibited only or cells became dead. Photomicrography reflects the type of cell death distinguished as apoptosis (shrinkage of cells, apoptotic bodies) or appearance of enlarged necrotic cells and necrotic bodies. Besides the qualitative aspects of results, individual images were subjected to quantitative analysis. Among the growth parameters, the quantification was extended to the measurements of a) the diameters of mother and daughter cells (given in μm), b) time of cell division (in min), duration of the cell cycle (in h), c) the number of vesicles of lysosomal digestion referred to as residual bodies and d) other growth parameters such as confluency and motility.

The production of classical time-lapse microscopy images is restricted even today to fluorescent and confocal microscopy as well as flow cytometry. However, these methods have their drawbacks relative to the TLS systems. Among the dyes of fluorescence microscopy, the carcinogenic compounds required increased attention. The disadvantage of confocal microscopy is that it needs expensive and high-precision instruments that not every lab or institution can afford. Other factors to be considered are the lack of physiological conditions, limiting the duration of observation in most cases to 24 h. The elapsed time between consecutive exposures usually is 1 min, and the selection of specimens for testing is also to be taken into consideration. Fixing agents can change the original structure, and artefacts may be generated. Further problems may arise from the phototoxic effect on cells or tissues, mainly when fluorescent methods are to be used.

An essential aspect of measuring cytotoxicity is that relative to the conventional methods, the MTT test, coupled with the TLS system is economical. The analysis of a single image allows the observations of several parameters. A further advantage of the combined analysis is that the results of TLS can be maintained up to one month, depending on the sample tested and data stored. The consecutive exposures of microphotography can be extended from 15 sec to 1 min. TLS exposures do not need human interference. The parameters of TLS are set after starting automatic recording, and the system is running until the footage is terminated. For the toxicology tests, the TLS system contains a 10x objective to visualize populations of cells, but no specific culture dishes are required. Physiological conditions for the detection by TLS are maintained inside the $CO_2$ incubator. The quantitative *in vitro* data obtained by TLS reduces the number of animals that would be sacrificed during *in vivo* experiments.

Our custom-built TLS system consists of an inverse microscope and a CCD camera built in the ocular tube.

Important additional accessories are near-infrared light-emitting diodes (LEDs, 960 nm) serving as light sources. The application of the near-infrared light source reduced the photo- and thermotoxicity to an undetectable low level (4). Cameras of microscopes are controlled by computers.

To test and validate our TLS system for its application *in vitro* toxicology, the well known antitumor agents 5-fluorouracil and methotrexate were selected as positive controls. The nucleoside analogue N-153 of unknown biological effects was also tested to prove that the method also applies to new antimetabolites.

## Materials and Methods

*N*-153 (1-[2'-Deoxy-2'-C-(n-propyl sulfanyl methyl)-3',5'-di-O-(tert-butyldimethylsilyl)-β-D-arabinofuranosyl]-uracil) was obtained from the Department of Pharmaceutical Chemistry, University of Debrecen (Hungary, Debrecen). The compound referred to as N-153 is a uridine-derived di-*O*-silylated nucleoside analogue featuring an unnatural D-arabinose sugar configuration and an n-propyl sulfanyl methyl branch at the C2' position. The compound was synthesized by photoinitiated addition of the thiyl radical generated from *n*-propanethiol onto the double bond of the corresponding uridine 2'-exomethylene derivative. The latter nucleoside exomethylene was obtained from uridine in three steps, including silylation of the 3'- and 5'-hydroxyl groups followed by subsequent oxidation and Wittig-olefination at C-2' position of the disilyl derivative. The characterization of agent N-153 and the details of synthesis have been reported (5). The investigations of antiproliferative activities of the new nucleoside derivative N-153 and 5-FU started with the MTT test. The structures of the two nucleoside analogues are given (Figure 1).

Due to the apolar character of the new N-153 analogue (Figure 1A), it was dissolved in 1% (v/v) DMSO. Based on our earlier observations, 1% (v/v) DMSO does not cause changes in the viability of cells at this dilution. The inhibition of N-153 exerted on the viability of cells in a relatively broad range of nucleoside analogue concentration (5-40 μg/ml) was measured three times in 8 parallel samples, each. This approach gave results to determine the inhibitory concentrations exerted on different cell lines.

*5-Fluorouracil.* The antineoplastic 5-fluorouracil (Figure 1B) is a well-known antimetabolite (6). It was purchased from Sigma-Aldrich, Budapest, Hungary. Under *in vivo* conditions, it is turning to 5-fluorouridine-monophosphate. Replacement of UMP with 5-fluorouridine monophosphate in the rRNA substrate did not affect the pre-rRNA processing (7). Its deoxynucleotide analogue, F-dUMP is an inhibitor of thymidylate synthase (8). Other fluorouracil derivatives are incorporated both into RNA and DNA exerting strong physiological effects and serving as useful antitumor agents against, colon, rectal, breast, stomach, pancreatic, ovary and liver cancers (9). As the liver is also subjected to heavy load during the treatment with fluorouracil derivatives, transitory elevation of serum aminotransferases may arise.

*Methotrexate* (MTX) is an antineoplastic, antimetabolite, antifolate agent with remarkable immunosuppressant potential (Figure 1C). The drug is broadly used against leukaemia, lymphoma, psoriasis and rheumatoid arthritis. MTX is a tetrafolate inhibitor preventing the enzymatic activity of the tetrahydrofolate-
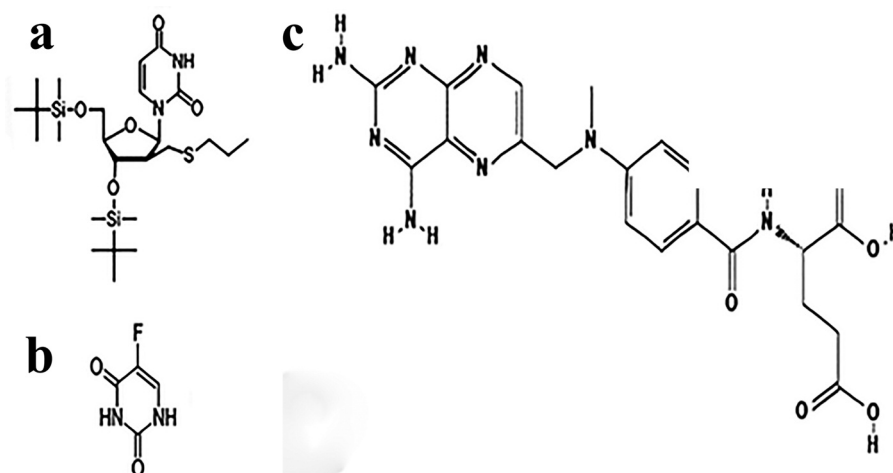
Figure 1. *2D structures of (a) N-153, a new uridine-derived di-O-silylated nucleoside, (1-[2'-deoxy-2'-C-(n-propylsulfanylmethyl)-3',5'-di-O-(tert-butyldimethylsilyl)-β-D-arabinofuranosyl]-uracil), (b) 5-fluorouracil, (c) methotrexate.*

dehydrogenase and preventing the formation of tetrahydrofolate necessary for the synthesis of thymidylate (10).

*Cell lines*. HaCaT cell line was derived from human skin, prone to spontaneous transformation *in vitro* during prolonged incubation. Cells were cultured in DMEM medium (Biocenter, Szeged, Hungary) containing 10% fetal bovine serum (FBS, Hyclon, Logan, UT) and 1% antibiotic-antimycotic mixture (Penicillin–Streptomycin–Neomycin). SCC-VII carcinoma cell line originally arose in the abdominal wall of C3H mice in Dr Herman Suit's laboratory at Harvard University, Boston, Massachusetts. SCC VII cells were grown in Dulbecco's Modified Eagle's Medium Nutrient Mixture (DMEM-HAM'S F12) (Sigma-Aldrich, Budapest, Hungary). The nutrient mixture was supplemented with two mM L-glutamine, 23 mM $NaHCO_3$, 100 U/ml penicillin, 100 U/ml streptomycin, 1% non-essential amino acids and 10% fetal bovine serum.

*CHO-K1 cell line*. In 1957, T. Puck received Chinese hamster ovary cells from the laboratory of the Boston Cancer Research Foundation and isolated the original strain registered as CHO-K1 (ATCC® CCL-61™) cell line (11-13). This cell line model is often used in medical and pharmaceutical research also to produce recombinant proteins. As an industrial cell line, it serves for the mass production of therapeutic proteins. From three to ten grams of recombinant proteins are constructed per culture. CHO-K1 is suitable for human use allowing posttranslational modifications of recombinant proteins that function in humans. This cell line requires proline due to the lack of the proline synthesizing genes, and to the block of the biosynthetic pathway that converts glutamic acid to glutamine gamma-aldehyde (11). CHO-K1 cells were grown in Ham's-F12 (Biocenter, Szeged, Hungary) supplemented with two mM L-glutamine, 23 mM $NaHCO_3$, 100 U/ml penicillin, 100 U/ml streptomycin, 1% non-essential amino acids and 10% fetal bovine serum.

*HeLa cell line*. The HeLa cell line is one of the oldest and most widespread human cell lines (14). It is widely used in biological research, also serving as a model cell line. Among other applications, the vaccine against epidemic poliovirus was developed using HeLa cells (15). The HeLa cell line is highly adaptive and proliferates, and due to its rapid *in vitro* mutagenesis, it is cultivation with extreme care. It is prone to contaminate other cell lines (16). HeLa cells were cultivated in RPMI-1640 medium (Sigma-Aldrich, Budapest, Hungary) containing 10% fetal bovine serum (FBS), (Hyclon, Logan, UT, USA) and 1% antibiotic-antimycotic mixture (Penicillin-Streptomycin-Neomycin).

*Determination of $IC_{50}$ values*. The $IC_{50}$ value of a compound is defined as the concentration that inhibits cell growth by 50% relative to the control. After the MTT test, the medium containing the inhibitor was removed, and 100 μl MTT solution was added to the cells. The plates were then incubated for two h at 37°C. The medium from the wells was then carefully aspirated, and MTT formazan dissolved with 100 μl of DMSO aided by gentle agitation on a shaker. After 10 min at room temperature, the absorbances were read at 570 nm by an automatic plate reader.

The percentage of viability reflecting the respiratory potential of the cell population in each well was expressed as absorbance of treated cells/absorbance of control cells) ×100. $IC_{50}$ values of tested agents were determined by Graphpad (Prism) semi-log line fitting (17).

The MTT test was performed after treatment and removal of inhibitors followed by the addition of 100 μl MTT solution to the cells. Data obtained with the MTT test are given in the Results section.

*Incubator*. A SANYO MCO18-AC (Wood Dale, IL, US) CO2 incubator was used with a back-side instrument port. Its chamber was modified to host four microscopes.

*Microscopes*. Olympus (Tokyo, Japan) upright microscopes were modified for inverted usage, and revolver turrets were installed to replace the original illumination. The charge-coupled device (CCD) camera boards were placed under the turrets, using the monocular adapter lower parts of Olympus Tokyo as housing. Specimen tables were unmodified, but the slide orientation mechanisms were removed. Ocular sockets were used for illuminators. Microscope

objectives: Carl Zeiss (Jena, Germany) plan achromatic objectives (×10: 0.25 NA) that were used to enable a broad field of view to be imaged. Cameras: High-sensitivity digital (SSC) camera. KPC EX-20H high-resolution camera (KT&C, Seoul, Korea) with a Sony ExView CCD sensor. Illumination intensity at F 1.2:0.003 lux High 900-1000 nM near-infrared range sensitivity. Native frame rate: 25 frames/s.

*Image capture and display*. Ten images were collected, each within a 5-s interval and averaged to minimize noise. The collection of images within 5-s is regarded as high time resolution. Long-term scan (LTS) system: Illumination was provided by diodes emitting light at 940nm (LED: 5-mm diameter; 1.2 V and 50 mA, driven at 5 V using a serial 82 Ohm resistor) were used to illuminate cells while minimizing heat and phototoxicity. The longer wavelength offered a deeper penetration (up to 3-mm thickness) and less light dispersion through the culture medium and the wall of the T-flask. The theoretical limit of resolution under our conditions using a 940-nm wavelength at 1.25 numerical aperture was 1.88 nm based on the Abbe equation. The original 5 mm spherical light-emitting diode (LED) head was used as a condenser for better reproducibility of the setup. Illuminators were centred and fixed with glue in ocular microscope tubes. The distance between the upper surface of the T-25 culture flask and the spherical ball head of the LED was 120 mm. Illumination of cells lasted only during image acquisition periods (~5 s per time point).

*Image analysis*
*Post-processing*. National Health Institute's ImageJ software was used to analyze the image sequences of the time-lapse video microscopy (18).
*a) Image restoration and noise reduction*
- RGB image sequences were converted to 8-bit grayscale images.
- Resulting image stacks were deflickered to eliminate transient brightness changes due to the low light camera auto gain. The Stack Deflicker calculates the average grey value for each frame and normalizes all exposures so that they have the same average grey level as a specified frame of the stack (19). This plugin is useful to remove the flickering that is caused by frame rates different from the frequency of AC used for the light-source that illuminated the screen.
- Contrast and brightness were equalized based on the stack (sequence) histogram at 0.4% of the pixels saturated.
- Fast Fourier-transformation and background subtraction: The background was reduced by bandpass filtering to exclude large structures down to 40 pixels and filtering small particles up to 3 pixels in size, and background extraction process using a rolling ball at a radius of 50 pixels.
- Subtracting background: Based on the concept of the 'rolling ball' algorithm described by Sternberg Stanley based on the assumption that the 2D grayscale image has a third dimension (height) creating a surface. A ball of a given radius is rolled over the bottom side of this surface; the hull of the volume reachable by the ball is the background to be subtracted.
*b) Segmentation*. Image sequences were thresholded using a stacked histogram by keeping the information containing elements of the image sequence as foreground and throwing the redundant pixels away by thresholding them into the background.
*c) Measurement*. Thresholding results in a binary image were used for graphical representation.

*Cell size measurements*. Divided cells were selected from the binary image sequence based on their circularity determined by area/perimeter ratio. Larger pre-division mother cells were separated from smaller post-division daughter cells. Pixel size was calibrated with a Burker chamber. Diameter calculation implied pixel to μm transformation.

*Determination of the time of cell division*. Cell division starts with the lifting up of mitotic mother cells and dividing. It lasts until daughter cells settle down and attach to the growth surface. The time of cell division was determined manually using the Orthogonal Views function of the Fiji program.

*Determination of generation time*. Images were acquired at a frame rate of 1 frame per minute. Two daughter cells of a dividing mother cell were followed in time until their next division, resulting in 2 pairs of new daughter cells.

## Results

*MTT assay*. Cell cultures were kept under the same conditions during the experiments. Cells were grown at 37°C, 95% humidity, and 5% $CO_2$ in the carbon dioxide incubator. After three days of incubation in cell culture flasks, cells were trypsinized, and homogeneous cell suspensions were formed. Aliquots (200 μl) of each cell suspension containing the inhibitor at the final concentration were placed in wells of 96-well-plates (Biocenter, Szeged, Hungary). During the MTT-assay, different starting cell numbers were used due to cell cycle differences; HaCaT were started at 10,000 cells/well, while SCC VII, CHO-K1, and HeLa cultures started at 5,000 cells/well. After subculturing, 24 h was allowed for the cells to adhere to the bottom of the wells. The experiments were performed in microtiter plates containing 96 wells.

According to our protocol, an aliquot of the desired final volume of medium is given first and pre-warmed in a water bath (typically for 15 min to equilibrate to 37°C) before adding the agent to be tested. Commonly, 200 μl of the medium is used per well of a 96-well plate. The medium and agent were mixed by suspension or vortexing. The agent was dissolved in 1% DMSO and diluted with prewarmed DMEM/DMEM-F12/Ham's F12/RPMI 1640 in 1% (v/v) DMSO concentration and placed it into the wells of plates. The cells were incubated for a further 48 h under the breeding conditions. The control sample contained only DMSO in a prewarmed medium. The following analogue concentrations were tested: 5, 10, 20, 30 and 40 μg/ml. The $IC_{50}$ values were determined using the equations given in Table I. The inhibitory concentration of N-153 was determined for each cell line (Table I). These data show a significant difference between the non-tumorous HaCaT and tumorous SCC cell lines, whereas the inhibitory concentrations of CHO-K1 and HeLa cells were practically the same (Figure 2).

Viability was tested at 5, 10, 20, 30, and 40 μg/ml concentrations of the 5-FU nucleoside analogue. Treatment

Table I. *IC$_{50}$ concentrations of N-153 in different cell lines.*

| N-153 | Semi-log equation | R$^2$ | IC$_{50}$ (µg/ml) |
|---|---|---|---|
| HaCaT | 50=239.1-193.2*log(x) | 0.9551 | 9.52 |
| SCC | 50=126.5-105*log(x) | 0.7509 | 5.35 |
| CHO-K1 | 50=149.5-124.2*log(x) | 0.8302 | 6.32 |
| HeLa | 50=147.7-123.1*log(x) | 0.8170 | 6.21 |

Table II. *IC$_{50}$ concentrations of 5-FU for different cell lines.*

| 5-FU | Semi-log equation | R$^2$ | IC$_{50}$ (µg/ml) |
|---|---|---|---|
| HaCaT | 50=91.47-36.45*log(x) | 0.8767 | 13.73 |
| SCC | 50=43.66-10.90*log(x) | 0.9041 | 0.26 |
| CHO-K1 | 50=80.60-30.57*log(x) | 0.9781 | 10.02 |
| HeLa | 50=56.34-17.13*log(x) | 0.8144 | 2.34 |

Table III. *IC$_{50}$ concentrations of 5-MTX in different cell lines.*

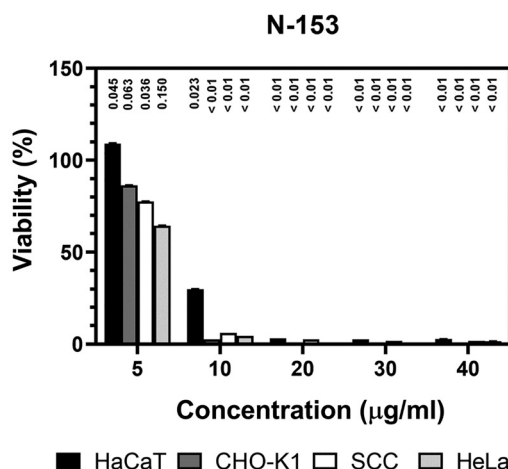| MTX | Semi-log equation | R$^2$ | IC$_{50}$ (µg/ml) |
|---|---|---|---|
| HaCaT | 50=52.20-7.08*log(x) | 0.8455 | 2.04 |
| SCC | 50=92.32-18.09*log(x) | 0.9568 | 218.48 |
| CHO-K1 | 50=150.1-44.7*log(x) | 0.9277 | 173.53 |
| HeLa | 50=49.10-7.094*log(x) | 0.9801 | 0.75 |



Figure 2. *MTT viability assay of N-153 on different cell lines. Viability was tested at 5, 10, 20, 30, and 40 µg/ml concentrations of the N-153 nucleoside analogue. Treatment lasted for 48 h. As the standard deviation values are minimal, they are given as numbers above the columns of viability.*

lasted for 48 h. Except for CHO-K1, the viability of other cell cultures fell below 50% upon treatment with five µg/ml 5-FU. Standard deviations are small, indicated by numbers above columns (Figure 3). The IC$_{50}$ values were determined using the equations of Table II. Viability of HaCaT and HeLa cells upon MTX was less than 50% even at the lowest MTX concentration. To the contrary, in CHO-K1 and SCC cells viability was higher than 50 % at the highest inhibitor concentration (Figure 4). Due to the small standard deviations, these values are given as numbers place above the measurements. The IC$_{50}$ values were determined using the equations (Table III).

IC$_{50}$ values of nucleoside analogues obtained by the MTT test presented (Tables I, II and III), served to follow cellular processes using time-lapse video microscopy. It was to be decided whether the cellular process suffered a drastic reduction of cell viability by the temporary disruption of the cell cycle, or cell death (apoptosis or necrosis) occurred. These questions could not be answered unanimously by the MTT test alone. We have grown each cell type at the IC$_{50}$ concentration corresponding to its nucleoside analogue.

*Quantification of long-term scanning.* Changes in the size of mother cells. The size of the mother cells was determined based on the relationship between diameter and volume (20). The standard curve contains data of measured diameters obtained by TLS and calculated volumes belonging to the diameters. We showed how the diameter-volume values changed in cell lines upon treatment of relative to the DMSO controls (Figure 5).

Cells were grown in medium containing 1% DMSO at their corresponding IC$_{50}$ concentrations of N-153 nucleoside analogue, and cellular changes were registered and given in %. Results are given as differences in percentages after treatment relative to the DMSO control (100%). N=30. Characteristic data of parameters are given by the average values of n=30 samples (Table IV). Changes in the size of cells may reflect cytotoxicity. Values are given in percentages relative to the DMSO controls. The size of HaCaT cells decreased by 19.71%, CHO-K1 by 16.20% and HeLa cells by 3.01% upon treatment with IC$_{50}$ concentration of N-153. On the other hand, the size of SCC cells after the treatment increased by 4.18%.

After treatment with 5-FU the cell size of HaCaT decreased by 22%, after treatment of CHO-K1 by 5.62, HeLa by 6.17 and SCC by 1.71%. Only the change caused by HaCaT cell size is considered significant. Cellular changes are given in percentages as treated – 5FU/ DMSO control (100%). Numbers of measurements: HaCaT n=18, SCC n=2, HeLa n=12. Upon treatment the HaCaT mother cell decreased by 5.83%, CHO-K1 2.45%, did not change in SCC cells, and increased by 7.3% in HeLa cells. Cellular
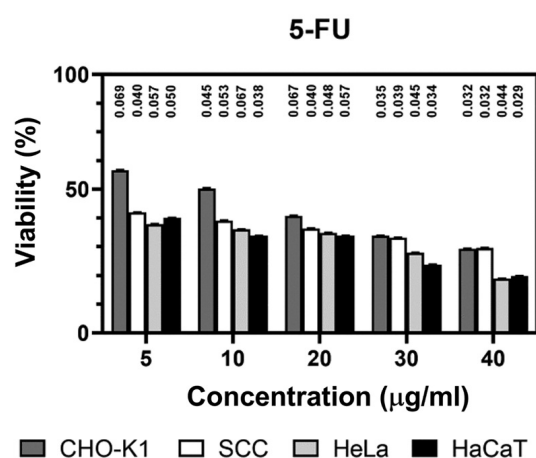
**5-FU**



**MTX**



Figure 3. *MTT viability assay of 5-FU on different cell lines. Viability was tested at 5, 10, 20, 30, and 40 µg/ml concentrations of the 5-FU nucleoside analogue. Treatment lasted for 48 h. Except for CHO-K1, the viability of other cell cultures fell below 50% upon treatment with 5 µg/ml 5-FU. Standard deviations are small, indicated by numbers above columns.*

Figure 4. *MTT viability assay of MTX on different cell lines. Viability was tested after treatment with 5, 10, 20, 30, and 40 µg/ml concentration of the MTX. Treatment lasted for 48 h.*

changes are given in percentages as treated - MTX/DMSO control (100%). HaCaT n=20, SCC n=20, HeLa n=12.

*Time of cell division.* Cells were grown in medium containing 1% DMSO at their corresponding $IC_{50}$ concentrations of inhibitors. Changes in cell division were registered and given in % (Table V). Results are differences in percentages after treatment relative to the DMSO control (100%) (N=30). Characteristic data of parameters are given by the average values of n=30 samples.

The time of cell division increased in each cell type after treatment with N-153 to varying degrees (Figure 6, Table VI). The time of cell division increased by 39.24% in HaCaT cells and only by 10% in SCC cells, reflecting that non-tumorous HaCaT cells are more vulnerable towards N-153 than the tumorous SCC cells. Other cell lines showed an increase in cell division, CHO-K1 13.65 and HeLa 11% similar to tumorous SCC cells.

Similarly to N-153, 5-FU impacted the time of cell division to different degrees. A significant increase was found in HaCaT (23.11%), SCC (100.44%) and HeLa (58.97%). Cellular changes are given in percentages as treated – 5FU/DMSO control (100 %). HaCaT n=18, SCC n=2, HeLa n=12. The time of cell division was higher in HaCaT cells (+8,24%), in CHO-K1 (+9.8%) and HeLa cells (+25.4%) but remained unchanged in SCC cells. Cellular changes are given in percentages as treated - MTX/ DMSO control (100%). HaCaT n=20, SCC n=20, HeLa n=10.
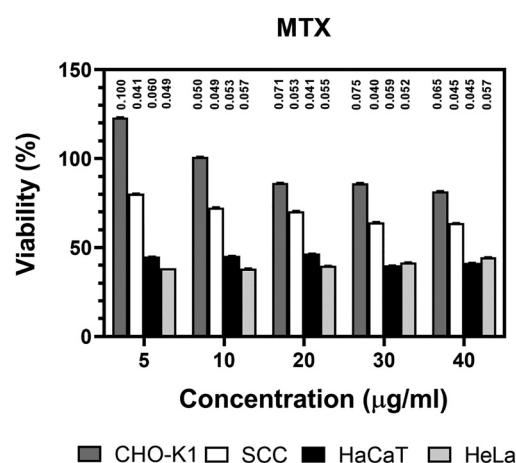
Table IV. *Changes in the size of mother cells in percentages at $IC_{50}$ concentrations.*

| Cell size before division (µm) change in % | N-153 | 5-FU | MTX |
|---|---|---|---|
| HaCaT | −9.57±1.44 | 22.06±0.66 | 5.83±0.61 |
| SCC | 4.18±0.88 | −1.71±0 | 0.27±1.45 |
| CHO-K1 | −16.20±1.14 | 5.67±1.01 | −2.45±6.27 |
| HeLa | −3.01±0.50 | 6.17±0.57 | 7.29±1.63 |

Table V. *Changes in time of cell division at $IC_{50}$ concentrations of antimetabolites.*

| Duration of cell division (min) relative to the control in % | N-153 | 5-FU | MTX |
|---|---|---|---|
| HaCaT | 39.24±8.26 | 23.11±12.65 | 8.24±14.52 |
| SCC | 10.20±7.44 | 100.44±16.56 | 0.73±4.87 |
| CHO-K1 | 13.65±4.92 | 5.65±7.12 | 9.76±5.98 |
| HeLa | 10.71±10.37 | 58.97±24.45 | 25.40±19.50 |

Table VI. *Changes in the duration of the cell cycle after treatment of N-153 at $IC_{50}$ concentration.*

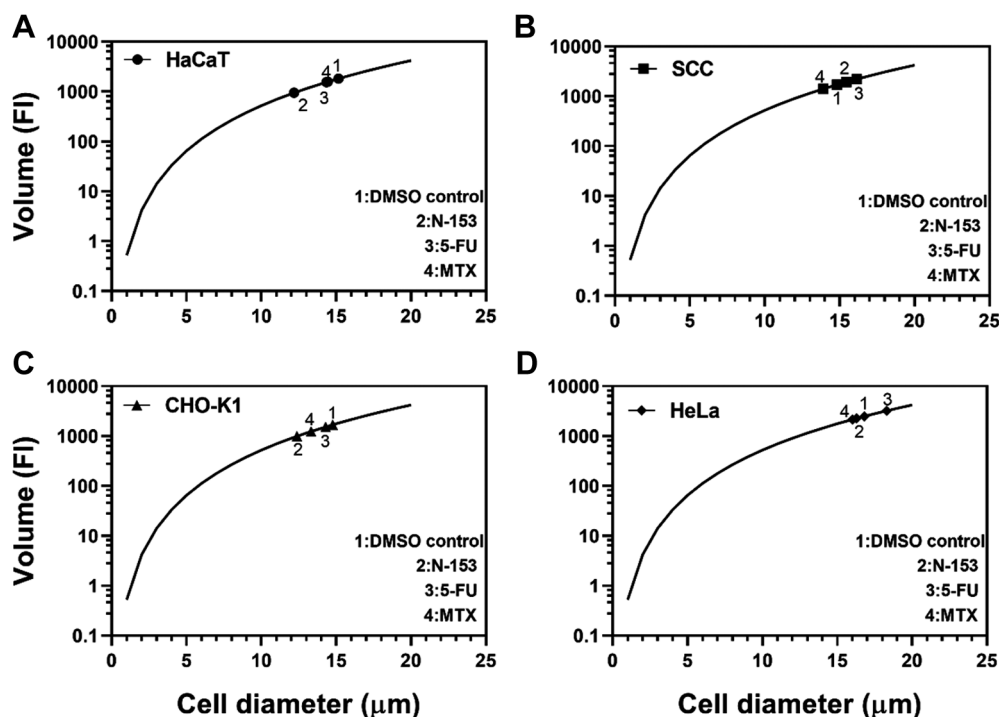| Duration of cell cycle (h) change in % | N-153 | 5-FU | MTX |
|---|---|---|---|
| HaCaT | 15.83±2.28 | 97.30±-1.68 | n.m. |
| SCC | 43.68±4.55 | n.m. | 38.46±2.75 |
| CHO-K1 | 48.03±4.78 | 55.81±5.84 | 1.41±1.40 |
| HeLa | 52.14±2.70 | n.m. | n.m. |

Figure 5. *Changes in cell diameter and cell volume. Cell diameter and volume were measured relative to the control, after treatment at $IC_{50}$ with N-15, 5-FU and MTX in (A) HaCaT, (B) SCC, (C) CHO-K1 and (D) HeLa cells.*

*Generation time.* Table VI contains changes in the duration of the cell cycle after N-153 treatment. Cells were grown in medium containing 1% DMSO at their corresponding $IC_{50}$ concentrations of N-153 nucleoside analogue, and cellular changes were registered and given in %. Results are given as differences in percentages after treatment relative to the DMSO control (100%). Characteristic data of parameters are given by the average values of n=30 samples. n.m.=not measurable. The change in the duration of the cell cycle also indicates cell toxicity. As opposed to times of cell division, the generation time of HaCaT cells increased only to a smaller extent after N-153 treatment, whereas in other cell lines a considerable increase was observed (Figure 7). In HaCaT cells, the cell-cycle increase was 15.83%, in SCC 43.68%. In HeLa cells, the generation times lasted nearly 50% longer than in control cells.

The generation time of tumor cell lines upon 5-FU treatment could not be determined. The length of the cell cycle of non-tumorous HaCaT cells was also significantly increased and almost doubled (97.3%) whereas the cell cycle of CHO-K1 increased by 55.81% following 5-FU treatment. Cellular changes are given in percentages as treated – 5FU/ DMSO control (100%). HaCaT n=4, SCC n=0, HeLa n=0. Changes in the generation time of HaCaT cells could not be

measured as daughter cell did not grow. Microphotographs show that cells did not divide and those cells that divided were immediately subjected to necrotic cell death. The proportion of cell growth was nearly 40% in SCC cells relative to the control. This growth can be accounted for by the cytostatic effect of MTX. The duration of CHO-K1 cells did not change, whereas the generation time of HeLa upon MTX treatment could not be determined as these cells lost their ability to attach to the matrix and were unable to divide or divided cells suffered necrotic cell death. Cellular changes are given in percentages as treated - MTX/ DMSO control (100%). HaCaT n=0, SCC n=15, HeLa n=0.

Similar experiments were carried out by others in keratinocytes treated with methotrexate (MTX). Increased cell size was observed after MTX treatment (21). Furthermore, it was noticed that the proliferation time was also extended in the tubular cells of the kidney by MTX (22). In human leukaemia cells, MTX caused unbalanced cell growth (23, 24) observed clonal synergistic inhibition upon combined treatment of colon and mammary tumours by MTX and 5-FU.

*Residual bodies of cell death.* There are two types of residual bodies generated during cell death, apoptotic bodies and necrotic bodies. These are not to be confused with residual
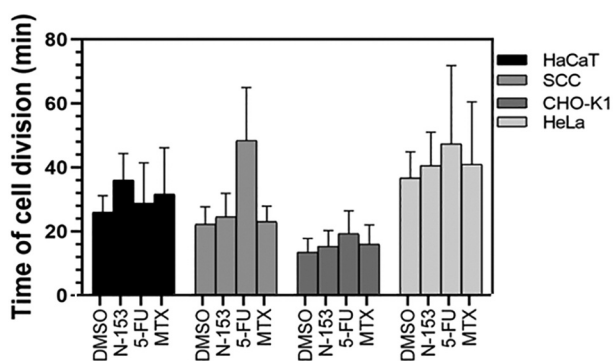
Figure 6. *Time of cell division (min). The diagram shows how the time of cell division changes after 48 h treatment of inhibitors relative to the DMSO control.*
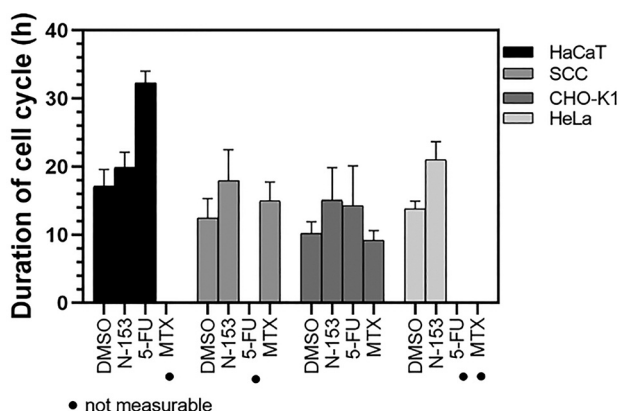


Figure 7. *Duration of the cell cycle (h). Changes upon 48 h treatment at $IC_{50}$ relative to the DMSO control are given. Black dots indicate missing data that could not be measured within 48 h.*

bodies secreted *via* exocytosis (that occurs in macrophages), or lipofuscin granules that remain in the cytosol indefinitely. Under conditions mentioned above, apoptotic and necrotic cells and their residual bodies can be identified and their parameters quantified by TLS. During the treatments with the two nucleoside analogues apoptosis was not observed but necrotic cells and their necrotic bodies became visible in the microphotographs. Low residual body counts were present in HaCaT and SCC cells, in contrast in CHO-K1 cells they were not present at all but generated in large quantities in HeLa cells upon treatment with N-153 nucleoside analogue (Figure 8).

Most necrotic bodies were formed by the end of 48 h 5-FU treatment in HaCaT cells. A CHO-K1 did not show residual body formation by 5-FU treatment. Residual bodies were present in low numbers in SCC and HeLa cells accountable, at least partially, by the inability to determine
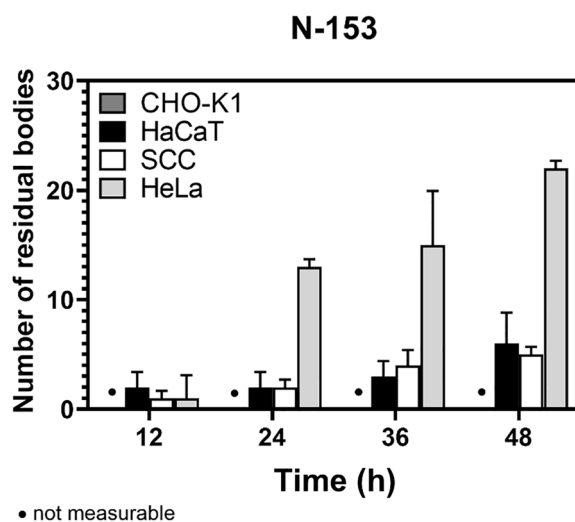


Figure 8. *Formation of necrotic bodies after N-153 treatment. The number of residual bodies in the visual field were counted during different times (12, 24, 36, 48 h) of incubation. After 12 h, no residual bodies were formed, but their number subsequently increased as the incubation continued. The most significant increase in the number of residual bodies occurred in HeLa cells.*

the cell cycle of these cell types. These observations are important because there was no change in the cell number of these recordings, consequently, in the diagrams below, only those residual bodies could be counted that were formed during the necrosis of cells.

*Formation and visualization of residual bodies.* In CHO-K1 culture, no residual body formation was observed (Figure 9). In other cell cultures, residual bodies appeared as a function of incubation time, and the number depended on the susceptibility of cell types to the nucleoside analogue. After the treatment of cell cultures with $IC_{50}$ concentration of 5-FU, the formation of residual bodies was tested (Figure 10). In CHO-K1 cells, residual bodies were undetectably low. Residual necrotic bodies were formed in other cell cultures as a function of incubation time, but in varying proportions with the highest number in HaCaT cells.

Similarly to N-153, the treatment of cells with 5-FU did not result in residual bodies in the CHO-K1 culture (Figure 11). Other cell culture's residual bodies contained their increasing number as a function of incubation time depending on the susceptibility of cell types on the 5-FU nucleoside analogue. The highest number of necrotic bodies formed after 48 h in HaCaT cells. Upon MTX treatment, necrotic bodies did not form in CHO-K1 cells (Figure 12). In SCC, HeLa and HaCaT cells necrotic bodies appeared 24h after MTX treatment and their number increased with time (Figure 13). The increasing number of necrotic bodies in
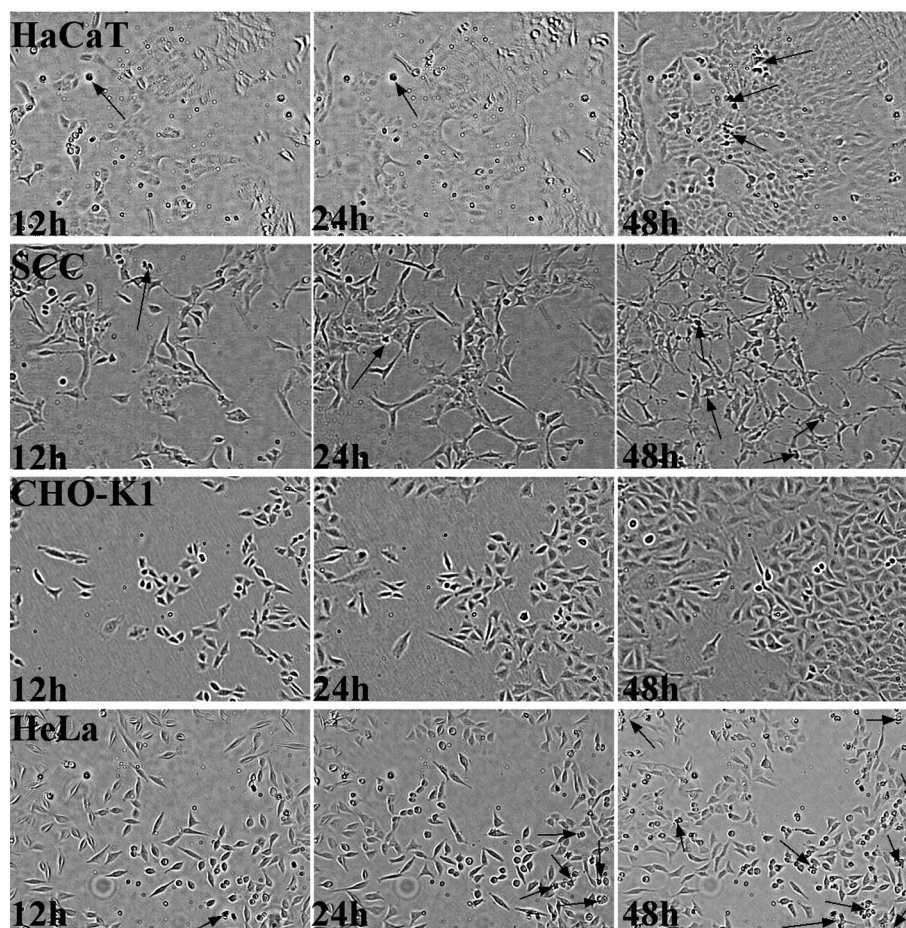
Figure 9. *Formation of residual bodies in cell cultures in the presence of N-153 as a function of time. Visualization of residual bodies took place during time-lapse microscopy treating cells with IC$_{50}$ concentration of N-153. Black arrows point to necrotic bodies.*

different cell lines expresses the sensitivity of cell lines to MTX in this order: CHO-K1 < SCC < HeLa < HaCaT.

## Discussion

Cancer is among the leading causes of death, and the number of cases is constantly growing worldwide. No wonder that the application of nucleoside derivatives and analogues as antitumor agents has significantly increased in the field of oncology. In the therapy of cancer patients nucleotides, nucleosides or base analogues account alone or in combination with other drugs for about 20% (25). Today there are about ten types of active substances belonging to this category used in tumour therapy, whereas the demand for such compounds is constantly increasing. Purine and pyrimidine analogues are present in clinical practice as antimetabolites. The macrolactam leinamycin produced by several Streptomyces atroolivaceus species possesses
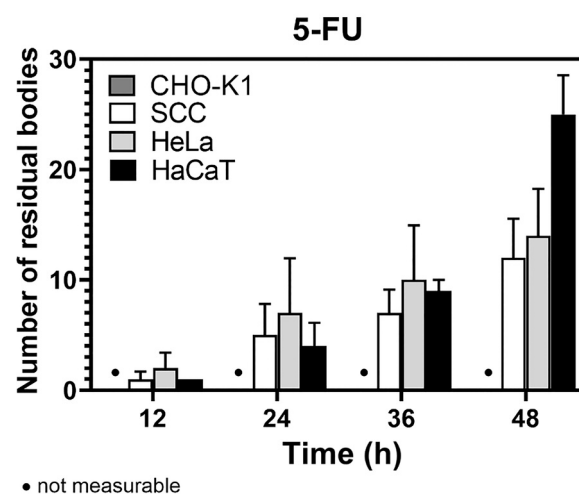


• not measurable

Figure 10. *Formation of residual bodies after 5-FU treatment. The number of residual necrotic bodies were counted that were formed during different incubation times (12, 24, 36, 48 h).*
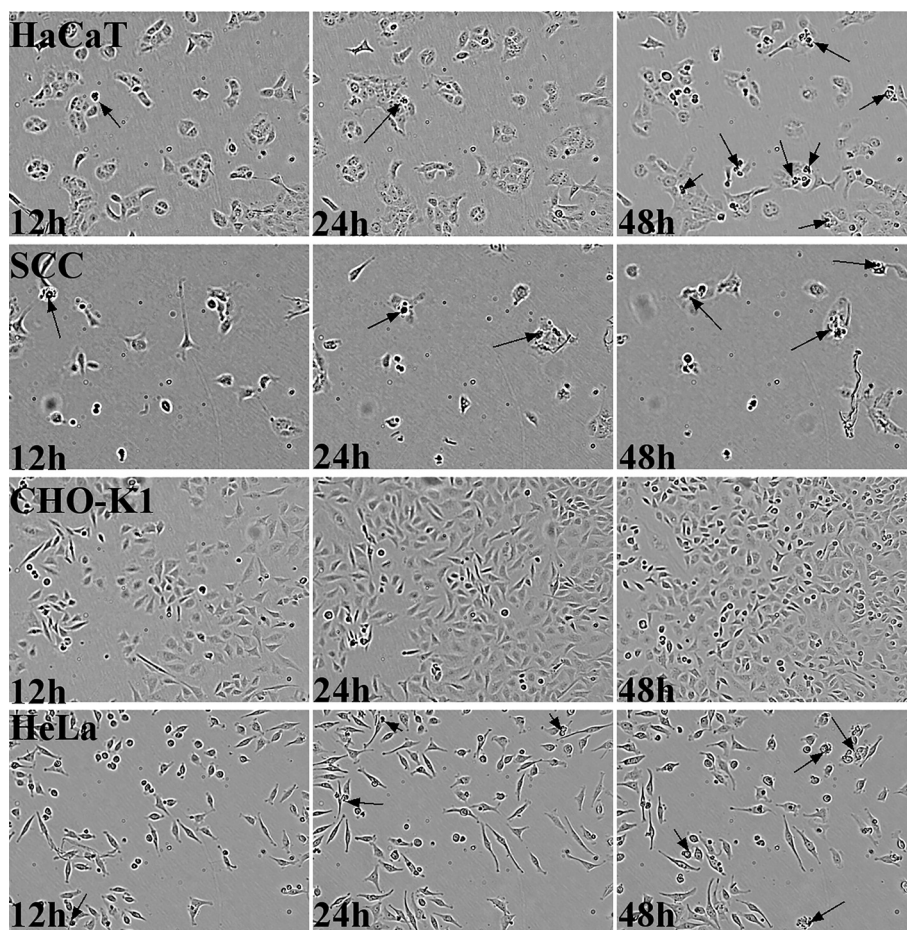
145

Figure 11. *Visualization of residual bodies in cell cultures in the presence of 5-FU as a function of time. Visualization of residual bodies took place during time-lapse microscopy, treating cells with $IC_{50}$ concentration of 5-FU. Black arrows point to necrotic bodies.*

remarkable antitumor and antibacterial properties due to its ability to inhibit DNA synthesis (26, 27). The analogues of leinamycin showed increased cytotoxic activity against HeLa tumour cells. Especially the lipophilic, silyl group-containing derivatives of leinamycin proved to be active (28).

Silyl- and trityl-modified nucleosides turned out to be more effective against tumour cell lines than nucleosides that were not modified. The lowest inhibitory concentration of silyl- and trityl-modified (5'-O- and 3',5'-di-O-) derivatives was ~25 μM (29). Among the candidates of the drug development are compounds that belong to the antitumor and antiviral sugar-modified nucleosides. The development of those nucleosides and nucleic acid analogues for tumour therapy was preferred that showed favourable chemical and biological properties. The replacement of oxygen in ribose by different elements such as sulfur, nitrogen or fluorine, resulted in new therapeutic analogues. As examples the 5'-thio nucleotide derivatives are mentioned that are inhibitors of essential enzymes of
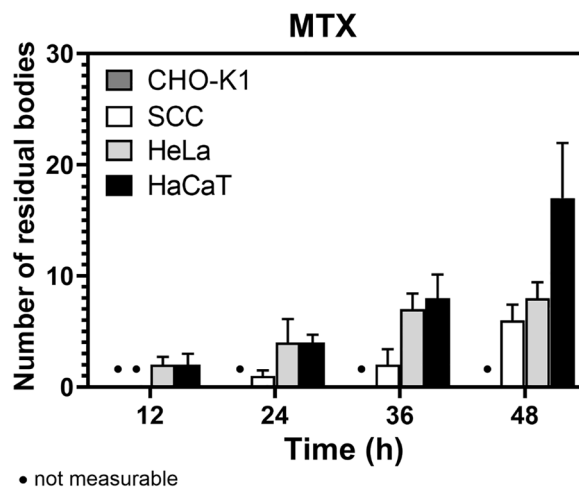


Figure 12. *Accumulation of residual bodies in cell cultures in the presence of MTX as a function of time. Visualization of residual bodies took place by time-lapse microscopy, treating cells with $IC_{50}$ concentration of MTX. Black arrows point to necrotic bodies.*
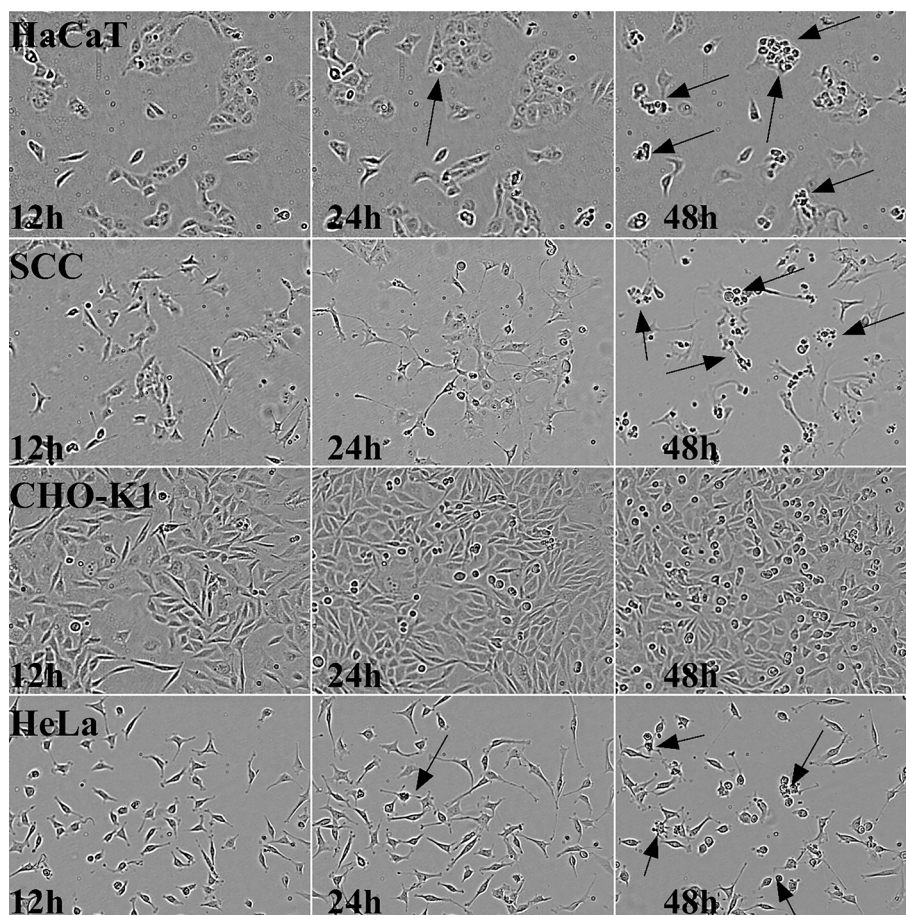
Figure 13. *Formation of residual bodies after MTX treatment. The number of residual necrotic bodies were counted that were formed during different incubation times (12, 24, 36, 48 h).*

nucleic acid biosynthesis, branched C2', C3' nucleosides show antitumor and antiviral activities (30, 31).

Other potentially active compounds of medicinal importance are nucleotides substituted with silicon (Si). These types of derivatives could result in useful biological compounds similar to their carbon-based forms, also possessing four valence electrons. Nevertheless, basic differences in the electronic makeup between C and Si atoms lead to substantially different physicochemical and pharmacokinetic properties. The Si-C bond length is significantly longer (C-Si, 186 pm) than the C-C bond (C-C, 154 pm), causing differences in the size and shape of Si and C containing analogues. The relatively longer bond distances of Si could result in the interaction of silicon-containing derivatives with special proteins. The bond distances could also explain why the pharmacological profiles are different from those of carbon-based derivatives. Due to the higher electropositivity of Si, the reduction, *i.e.* losing an electron and forming a positive ion is higher than that of carbon.

In general, the lipophilic character of silicon is more expressed than its carbon variant. By raising the lipophilic character, the effectivity of introducing chemicals into tissues can be increased. This will impact the metabolic activity of the liver and the plasma half-life time relative to the non-silylated variant. The lipophilic character contributes to the faster crossing of a drug candidate molecule through the blood-brain barrier (32).

## Conclusion

The $IC_{50}$ values of N-153 were nearly identical in CHO-K1 and HeLa cells. During the quantification of results by time-lapse video microscopy following treatment at the $IC_{50}$ concentrations of N-153 nucleoside analogue, the size of cells, the time of cell division and the time of generation changed significantly relative to the DMSO control. HeLa cells were the most susceptible to the N-153 nucleoside analogue and increased above parameters as well as the number of residual

necrotic bodies in a time- and concentration-dependent manner relative to the DMSO control.

5-FU decreased the viability of cell cultures at lower concentrations than N-153. MTT test showed that the viability of cells at five µg/ml 5-FU was reduced by 60% with the notable exception of CHO-K1 cells. In HaCaT, SCC, and HeLa cells, the $IC_{50}$ values were lower than five µg/ml. Video Microscopic quantification showed that tumorous cell lines (SCC, HeLa) are more susceptible to 5-FU than the non-tumorous HaCaT keratinocyte cell line. Necrotic cell death was characteristic of 5-FU treatment except for CHO-K1 cells where necrotic residual bodies could not be seen in TLS images. In contrast to this observation in HaCaT, SCC and HeLa cells necrotic residual bodies appeared in a time- and concentration-dependent manner after 5-FU treatment.

Experiments also revealed that MTX decreased the viability to a lesser extent than N-153 or 5-FU. Another notable observation to mention is the high $IC_{50}$ value of CHO-K1 cells in contrast to HaCaT and HeLa cells, which conforms with the necrotic body formation in these cell lines.

To summarize the importance of this study, the MTT test was combined with time-lapse microscopy at the corresponding $IC_{50}$ concentrations characteristic to individual cancer cell lines. Time-lapse microscopy provided the following additional information besides the viability of cells upon treatment with the treatment of nucleoside analogue inhibitors, including changes in:
1. Cell size
2. Time of division into daughter cells (cytokinesis)
3. Duration of cell cycle
4. Degree of cell death (if any)
5. Type of cell death (apoptosis, necrosis)

The MTT test provided information related to the degree of inhibition of the cytotoxic agent, irrespective of whether cells remain alive or suffer cell death. The supplementation of the MTT test with time-lapse microscopy adds valuable visual information and allows the quantitative analysis of images of photomicroscopy. The microscopy and image analysis can be maintained for an extended period up to several weeks and widens the horizon of cellular toxicology tests. The perspectives of the combined analysis include, among others the cytotoxicity aspects of inhibitors of antimetabolic, antifungal and anticancer agents.

## Conflicts of Interest

## Authors' Contributions

## References

1 Farkas E, Ujvarosi K, Nagy G, Posta J and Banfalvi G: Apoptogenic and necrogenic effects of mercuric-acetate on the chromatin structure of K562 human erythroleukemia cells. Toxicol In Vitro *24(1)*: 267-275, 2010. PMID: 19723577. DOI: 10.1016/j.tiv.2009.08.021

2 Grela E, Kozłowska J and Grabowiecka A: Current methodology of MTT assay in bacteria - A review. Asta Histichem *120(4)*: 303-311, 2018. PMID: 29606555. DOI: 10.1016/j.acthis.2018.03.007

3 Palamakula A and Khan MA: Evaluation of cytotoxicity of oils used in coenzyme Q10 Self-emulsifying Drug Delivery Systems (SEDDS). Internat J Pharm *273(1-2)*: 63-73, 2004. PMID: 15010131. DOI: 10.1016/j.ijpharm.2003.10.010

4 Nagy G, Hennig GW, Petrenyi K, Kovacs L, Pocsi I, Dombradi V and Banfalvi G: Time-lapse video microscopy and image analysis of adherence and growth patterns of Candida albicans strains. Applied Microbiol Biotechnol *98(11)*: 5185-5194, 2014. PMID: 24691869. DOI: 10.1007/s00253-014-5696-5

5 Bege M, Bereczki I, Herczeg M, Kicsak M, Eszenyi D, Herczegh P and Borbas A: A low-temperature, photoinduced thiol–ene click reaction: a mild and efficient method for the synthesis of sugar-modified nucleosides. Org Biomol Chem *15(43)*: 9226-9233, 2017. PMID: 29085940. DOI: 10.1039/c7ob02184d

6 Benson AB: Gastrointestinal oncology. *In*: Springer Science and Business Media. Benson AB (ed). Dordrecht, pp. 294, 2012. DOI: 10.1007/978-3-642-13306-0

7 Ghoshal K and Jacob ST: Specific inhibition of pre-ribosomal RNA processing in extracts from the lymphosarcoma cells treated with 5-fluorouracil. Cancer Res *54(3)*: 632-636, 1994. PMID: 8306322.

8 Liu L and Santi DV: 5-Fluoro-2'-deoxycytidine 5'-monophosphate is a mechanism-based inhibitor of thymidylate synthase. Biochim Biophys Acta *1209(1)*: 89-94, 1994. PMID: 7947987. DOI: 10.1016/0167-4838(94)90141-4

9 Wecker L, Benz DA, Theobald RJ Jr: Brody's Human Pharmacology. *In*: Elsevier Health Sciences. Sixth edition, E-Book, Philadelphia, PA., pp 593, 2018.

10 National Center for Biotechnology Information. PubChem Database. Methotrexate, CID=126941. Available at: https://pubchem.ncbi.nlm.nih.gov/compound/Methotrexate [Last accessed on 22nd January 2020]

11 Lewis NE, Liu X, Li Y, Nagarajan H, Yerganian G, O'Brien E, Bordbar A, Roth AM, Rosenbloom J, Bian C, Xie M, Chen W, Li N, Baycin-Hizal D, Latif H, Forster J, Betenbaugh MJ, Famili I, Xu X, Wang J and Palsson BO: Genomic landscapes of Chinese hamster ovary cell lines as revealed by the Cricetulus griseus draft genome. Nat Biotech *31(8)*: 759-765, 2013. PMID: 23873082. DOI: 10.1038/nbt.2624

12 Wurm FM and Hacker D: First CHO genome. Nat Biotechnol 29(8): 718-720, 2011. PMID: 21822249. DOI: 10.1038/nbt.1943

13 Xu X, Nagarajan H, Lewis NE, Pan S, Cai Z, Liu X, Chen W, Xie M, Wang W, Hammond S, Andersen MR, Neff N, Passarelli B, Koh W, Fan HC, Wang J, Gui Y, Lee KH, Betenbaugh MJ, Quake SR, Famili I, Palsson BO and Wang J: The genomic sequence of the Chinese hamster ovary (CHO)-K1 cell line. Nat Biotechnol *29(8)*: 735-741, 2011. PMID: 21804562. DOI: 10.1038/nbt.1932

14 Beskow LM: Lessons from HeLa Cells: The ethics and policy of biospecimens. Annu Rev Genomics Hum Genet *17*: 395-417, 2016. PMID: 26979405. DOI: 10.1146/annurev-genom-083115-022536

15 Landry JJM, Pyl PT, Rausch T, Zichner T, Tekkedil MM, Stütz AM, Jauch A, Aiyar RS, Pau G, Delhomme N, Gagneur J, Korbel JO, Huber W and Steinmetz LM: The genomic and transcriptomic landscape of a HeLa cell line. G3 (Bethesda) *3(8)*: 1213-1224, 2013. PMID: 23550136. DOI: 10.1534/g3.113.005777

16 Rahbari R, Sheahan T, Modes V, Collier P, Macfarlane C and Badge RM: A novel L1 retrotransposon marker for HeLa cell line identification. Biotechniques *46(4)*: 277-284, 2009. PMID: 19450234. DOI: 10.2144/000113089

17 Prism 8 Curve Fitting Guide, Equation: Fitting a straight line on a semi-log or log-log graph. Available at: https://www.graphpad.com/guides/prism/8/curve-fitting/reg_fitting_lines_to_semilog.htm [Last accessed on 22nd September 2020]

18 ImageJ User Guide 2012. Adjust. Available at: https://imagej.nih.gov/ij/docs/guide/146-28.html#toc-Subsection-28.2 [Last accessed on 22nd September 2020]

19 ImageJ Plugins, Stack Deflicker. Available at: http://www.phage.dk/plugins/deflicker.html [Last accessed on 22nd September 2020]

20 Schwartz A, Sugg H, Ritter T and Fernandez-Repollet E: Direct determination of cell diameter, surface area, and volume with an electronic volume sensing flow cytometer. Cytometry *3(6)*: 456-458, 1983. PMID: 6851794. DOI: 10.1002/cyto.990030613

21 Schwartz PM, Barnett SK, Atillasoy ES and Millstone LM: Methotrexate induces differentiation of human keratinocytes. Proceed Natl Academy Sci *89(2)*: 594-598, 1992. PMID: 1731329. DOI: 10.1073/pnas.89.2.594

22 Grönroos M, Chen M, Jahnukainen T, Capitanio A, Aizman RI and Celsi G: Methotrexate induces cell swelling and necrosis in renal tubular cells. Pediatr Blood Cancer *46(5)*: 624-629, 2006. PMID: 16025437. DOI: 10.1002/pbc.20471

23 Taylor IW and Tattersall MH: Methotrexate cytotoxicity in cultured human leukemic cells studied by flow cytometry. Cancer Res *41(4)*: 1549-1558, 1981. PMID: 6163527.

24 Benz C, Schoenberg M, Choti M and Cadam E: Schedule-dependent cytotoxicity of methotrexate and 5-fluorouracil in human colon and breast tumour cell lines. J Clin Invest *66(5)*: 1162-1165, 1980. PMID: 7430346. DOI: 10.1172/JCI109946

25 Shelton J, Lu X, Hollenbaugh JA, Cho JH, Amblard F and Schinazi RF: Metabolism, biochemical actions, and chemical synthesis of anticancer nucleosides, nucleotides, and base analogues. Chem Rev *116(23)*: 14379-14455, 2016. PMID: 27960273. DOI: 10.1021/acs.chemrev.6b00209

26 Hara M, Saitoh Y and Nakano H: DNA strand scission by the novel antitumor antibiotic leinamycin. Biochem *29(24)*: 5676-5681, 1990. PMID: 2383554. DOI: 10.1021/bi00476a005

27 Asai A, Hara M, Kakita S, Kanda Y, Yoshida M, Saito H and Saitoh Y: Thiol-mediated DNA alkylation by the novel antitumor antibiotic leinamycin. J Am Chem Soc *118(28)*: 6802-6803, 1996. DOI: 10.1021/ja960892w

28 Szilagyi A, Fenyvesi F, Majercsik O, Pelyvas IF, Bacskay I, Feher P, Varadi J, Vecsernyes M and Herczegh P: Synthesis and cytotoxicity of leinamycin antibiotic analogs. J Med Chem *49(18)*: 5626-5630, 2006. PMID: 16942037. DOI: 10.1021/jm060471h

29 Panayides JL, Mathieu V, Moreno Y, Banuls L, Apostolellis H, Dahan-Farkas N, Davids H, Harmse L, Rey MEC, Green IR, Pelly SC, Kiss R, Kornienko A and van Otterlo WAL: Synthesis and *in vitro* growth inhibitory activity of novel silyl-and trityl-modified nucleosides. Bioorg Med Chem *24(12)*: 2716-2724, 2016. PMID: 27157005. DOI: 10.1016/j.bmc.2016.04.036

30 Bege M, Kiss A, Kicsák M, Bereczki I, Baksa V, Király G, Szemán-Nagy G, Szigeti MZ, Herczegh P and Borbás A: Synthesis and cytostatic effect of 3'-deoxy-3'-C-sulfanylmethyl nucleoside derivatives with d-xylo configuration. Molecules *24(11)*: 2173, 2019. PMID: 31185601. DOI: 10.3390/molecules24112173

31 Guinan M, Benckendorff C, Smith M and Miller GJ: Recent advances in the chemical synthesis and evaluation of anticancer nucleoside analogues. Molecules *25(9)*: 2050, 2020. PMID: 32354007. DOI: 10.3390/molecules25092050

32 Mills JS and Showell GA: Exploitation of silicon medicinal chemistry in drug discovery. Expert Opinion Invest Drugs *13(9)*: 1149-1157, 2004. PMID: 15330746. DOI: 10.1517/13543784.13.9.1149